

Observations on a cavitating trailing vortex behind a control surface

J.A. Venning¹, M.T. Khoo^{1,2}, B.W. Pearce¹ and P.A. Brandner¹

1 Cavitation Research Laboratory, University of Tasmania, Australia

2 Maritime Division, Defence Science and Technology Group, Australia

Abstract

Cavitation is the vapourisation of water which may occur about control or propulsive surfaces on marine platforms. Acoustic and photographic measurements have been made of the flow about a hydrofoil under various cavitation conditions. The development of the cavity is described, and quantitative measurements of the diameter variation with incidence are given. The twist in the cavity profile is shown to be stable in time. Acoustic measurements reveal the peak cavitating frequency to be a function of the hydrofoil incidence. Inception of the trailing vortex causes a 3 dB increase in the acoustic level, and leading-edge cavitation causes a further 5 dB increase. These measurements aid in understanding the physics of vortex cavitation.

I. INTRODUCTION

Cavitation is the process of pressure-induced phase-change from liquid to vapour that typically occurs in low pressure turbo-machinery flows (figure 1). Once vapour cavities form they may also contain incondensable gas via diffusion of dissolved gas from the liquid to vapour phase. The void in the fluid is filled with water vapour and some incondensable gas. It is generally a detrimental phenomenon, with undesirable effects such as decreased efficiency, increased noise production, and unsteady loads (Venning *et al.*, 2018a) that contribute to fatigue and vibration. A good understanding of cavitation behaviour is imperative to maximise the performance of marine platforms. The principal concern is to accurately predict cavitation inception,

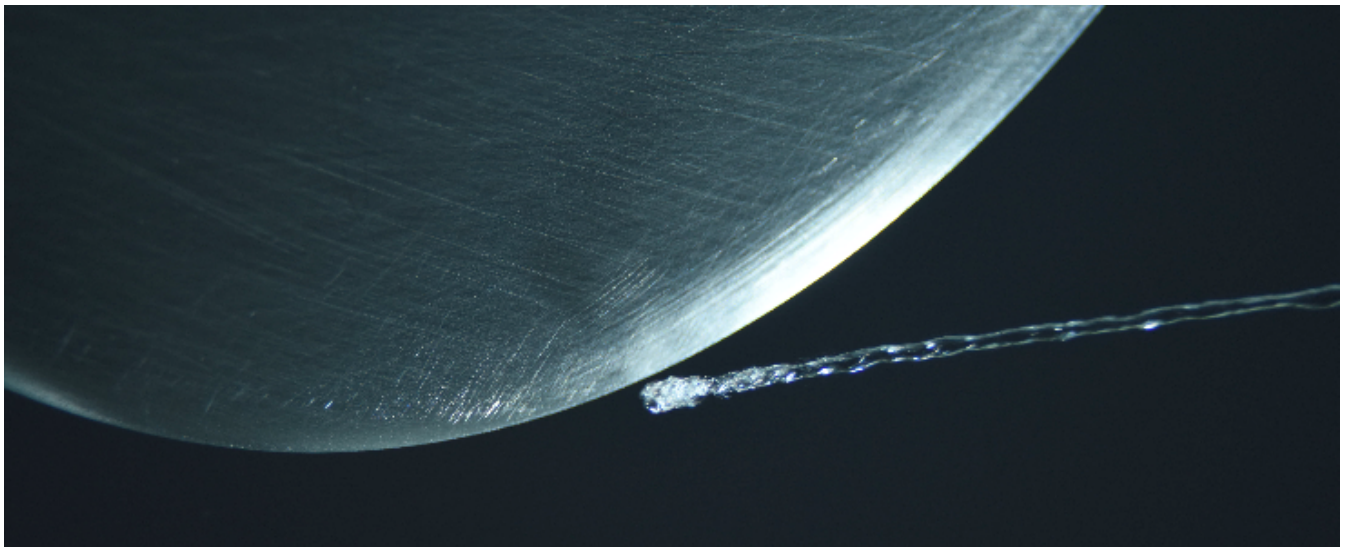


Figure 1: Photograph of the tip of a hydrofoil with a cavitating trailing vortex.

which is primarily dependent on the force produced by the propulsor, the depth of operation, and the 'quality' of the water. The quality describes the nuclei content of the water, which determines how much tension can be applied to the water before rupturing. Nuclei, which control the nucleation of phase change, are impurities such as microbubbles, solid particles (Brennen, 2014), or biological elements. These may reduce the strength of the water, making it more susceptible to cavitation (Brandner *et al.*, 2018).

In order to characterise the cavitation performance of marine propulsors and appendages, physical models can be tested in suitable hydrodynamic facilities such as cavitation tunnels. A cavitation tunnel generally consists of a recirculating body of water where the operating condition of a prototype can be altered and the cavitation behaviour observed. Water in these facilities may contain only sparse nuclei (Venning *et al.*, 2018b) or may be heavily seeded with bubbles, while water in the ocean is generally abundant with microbubbles (Shen & Gowing, 1986; O'Hern *et al.*, 1988; Gindroz *et al.*, 1995). Furthermore, cavitation or air ingestion can result in additional nuclei generation (Russell *et al.*, 2016). As such, care must be taken in controlling or monitoring the nuclei population during cavitation testing.

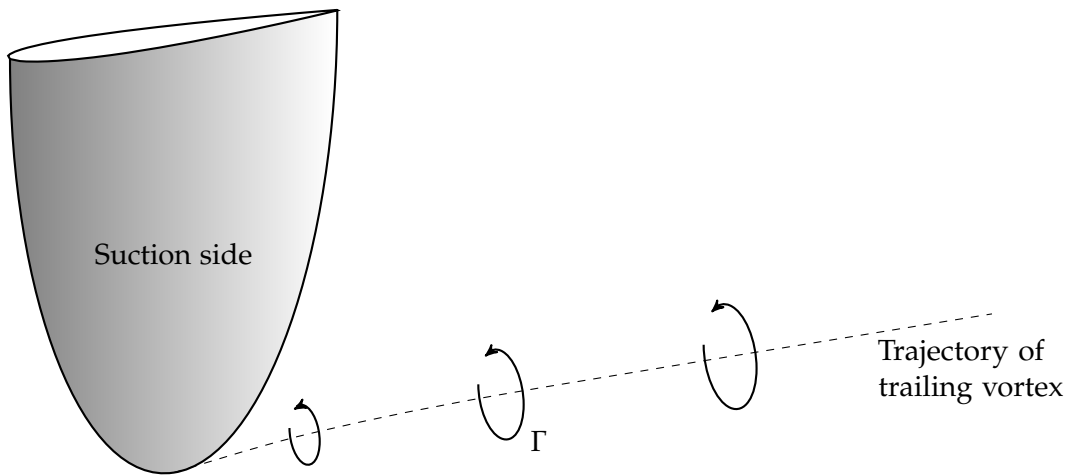


Figure 2: Schematic showing the trajectory and direction of rotation in a trailing vortex.

A hydrofoil is an ideal model of a control surface or a propulsor (Arndt, 2002). In producing lift, the hydrofoil generates vorticity, which is transformed into a concentrated trailing vortex (figure 2). The vortex persists many chord-lengths downstream due to low viscous dissipation. Microbubbles are ingested into this vortex, drawn by the lower pressure toward the core. As such, these vortices are often the most susceptible to cavitation. The strength of the trailing vortex increases as the hydrofoil produces more lift. These two factors are described by the circulation (Γ) and the lift coefficient (C_L). The lift coefficient describes the loading on the hydrofoil and is defined as:

$$C_L = \frac{L}{\frac{1}{2}\rho U_\infty^2 S}, \quad (1)$$

where L is the lift force, ρ the water density, U_∞ the freestream velocity and S the planform area of the hydrofoil. Beyond the loading of the hydrofoil, the primary non-dimensional quantities of interest are the Reynolds number (Re) and the cavitation number (σ). The cavitation number describes the likelihood and scale of any cavitation, and is defined as:

$$\sigma = \frac{p_\infty - p_v}{\frac{1}{2}\rho U_\infty^2}, \quad (2)$$

where p_∞ is the freestream static pressure and p_v the vapour pressure. The cavitation number was 1.0 for the current work. The Reynolds number describes the physical scales of the fluid compared to the viscous scales, and is defined as:

$$Re = \frac{U_\infty c}{\nu}, \quad (3)$$

where c is the root chord of the hydrofoil and ν the kinematic viscosity of the water. The Reynolds number was maintained at 2×10^6 for this study.

In this study, the results of cavitation testing on a generic hydrofoil are presented. The cavitation behaviour is described for various loading conditions on the hydrofoil. Measurements of the size of the cavitating vortex are given. The acoustics of the resulting cavitation are quantified through noise spectra.

II. EXPERIMENTAL SETUP

The Cavitation Research Laboratory's variable-pressure water tunnel (figure 3) at the Australian Maritime College was used for these experiments. The tunnel test section is 0.6 m square by 2.6 m long in which the operating velocity and absolute pressure ranges are 2 m/s to 13 m/s and 4 kPa to 400 kPa, respectively. The tunnel volume is 365 m³ with demineralised water as the working fluid. The tunnel has ancillaries for continuous injection and separation of microbubbles or large quantities of incondensable gas and for controlling the dissolved gas content. Microbubbles may be either injected for modelling cavitation nucleation or generated by the cavitation itself about experimental models. Microfluidic devices utilising cavitation at micrometre scales have been developed for generating high concentrations of microbubbles (Giosio *et al.*, 2016; Venning *et al.*, 2016; Russell *et al.*, 2018). Arrays of these devices enable the test flow to be seeded with polydisperse nuclei populations with a dominant size of about 15 μm to give concentrations in the water tunnel ranging from 0.1 /mL to 100 /mL. This feature allows for the measurement of cavitation performance

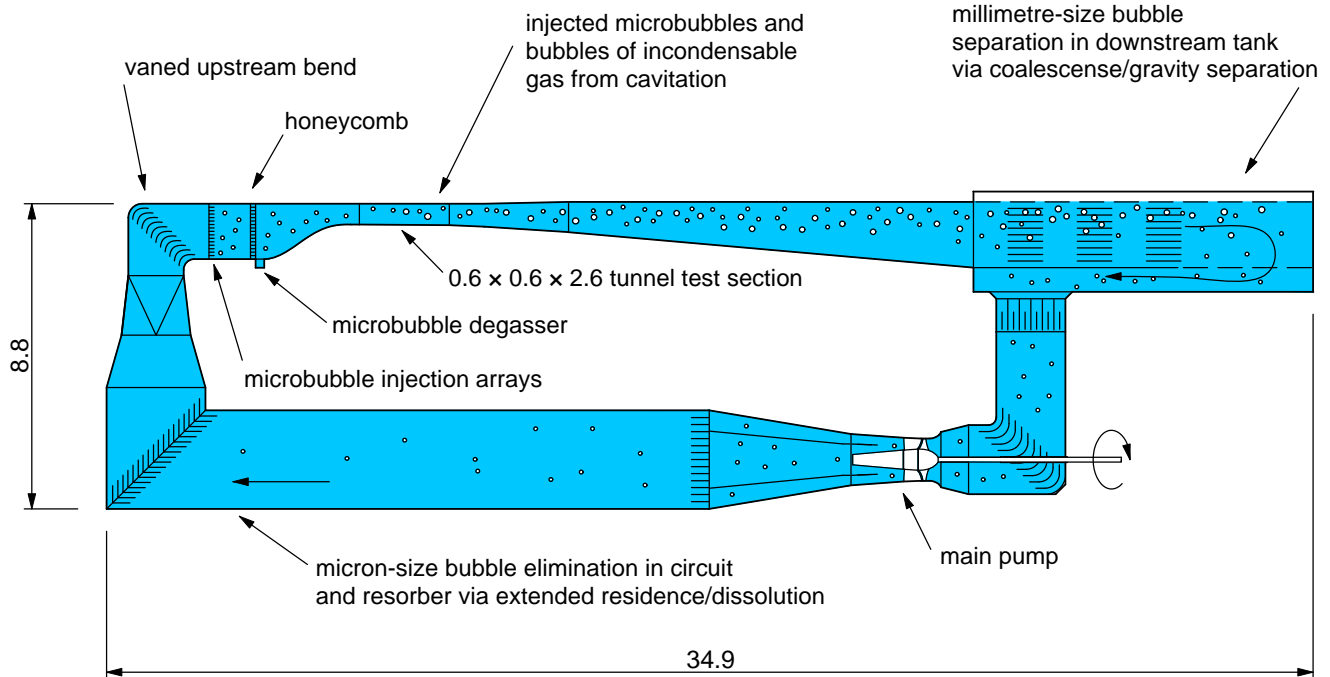


Figure 3: Schematic of the variable-pressure water tunnel showing the circuit architecture for continuous removal of microbubbles or large volumes of injected incondensable gas and ancillaries for microbubble seeding and for degassing of water. Microbubbles may be either injected for modelling cavitation nucleation or generated by the cavitation itself. All dimensions are in metres.

of a component across a range of water qualities. The tunnel water has a natural background nuclei population which is measured using a cavitation susceptibility meter as described by *Khoo et al. (2016)*. This population is sparse and has high strength (figure 4), so is only active in low cavitation number flows. Long duration measurements (*Venning et al., 2018b*) have shown this to follow a power law. Only the background nuclei population was used for the present experiments. *Khoo et al. (2018)* describes acoustic measurements of trailing-vortex cavitation in a flow abundant with nuclei.

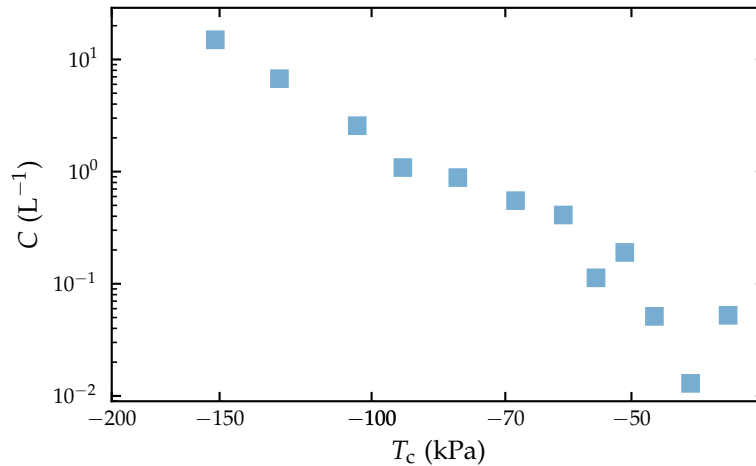


Figure 4: Nuclei content of the water expressed as a concentration against strength of the nuclei (defined as the difference between nucleus critical pressure and vapour pressure).

The elliptical planform stainless steel model has a NACA-0012 profile, root chord length of 150 mm, and a half-span of 176.7 mm. It was mounted to the test-section ceiling (figure 5) 1.3 m from the test-section entrance.

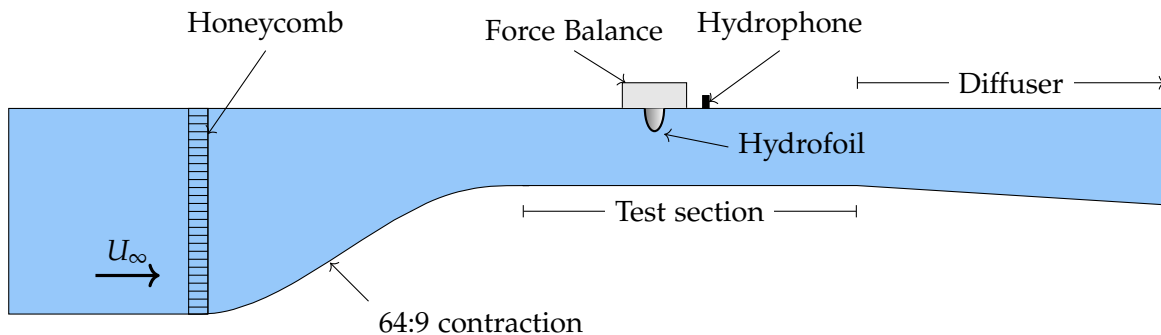


Figure 5: Schematic of experimental setup showing the hydrofoil location within the test section.

The cavitation behaviour was monitored using several methods. Acoustic measurements were recorded with a B&K type 8103 hydrophone mounted in the test-section ceiling, $2.5c$ (root chord lengths) downstream of the hydrofoil mid-chord. The unsteady pressure signals were amplified with a B&K Nexus conditioning amplifier type 2692, and acquired at 204.8 kHz for 20 s. These signals were decomposed into the frequency domain with a Welch algorithm (*Welch, 1967*) utilising a 2^{16} point Hanning window (0.32 s) with a 50% (0.16 s) overlap. Photographs were taken using a DSLR camera (Nikon D810) and stroboscopic lights.

III. RESULTS

The symmetric hydrofoil at zero-incidence created no trailing vortex. As the incidence increased, lift was produced by the hydrofoil, and a trailing vortex was formed. The pressure drop in the vortex increased with incidence, until the incidence was such that the minimum pressure in the flow was below vapour pressure. From this incidence onwards, the fluid was susceptible to cavitation, as tension was now applied to the fluid. However, inception will not occur until a nucleus with a strength less than the applied tension is captured by the vortex. The inception process is thus a function of the vortex state as well as the nuclei content of the water.

The development of the trailing vortex post inception with increasing incidence is demonstrated in the set of photographs in figure 6. Inception occurred at an incidence of 5.9° , and formed a long, thin tube of water vapour, with a bulbous head. At this incidence, the trajectory of the cavitating vortex was stable in time, though the streamwise location of the head ranged between $x/c = 0.086$ to $x/c = 0.105$ with an average of $x/c = 0.097$. These measurements correspond to physical dimensions of 12.9 mm to 15.8 mm behind the tip and an average of 14.5 mm. The bulbous head had an average diameter of 1.18 mm, length of 2.59 mm and an aspect ratio of 2.2.

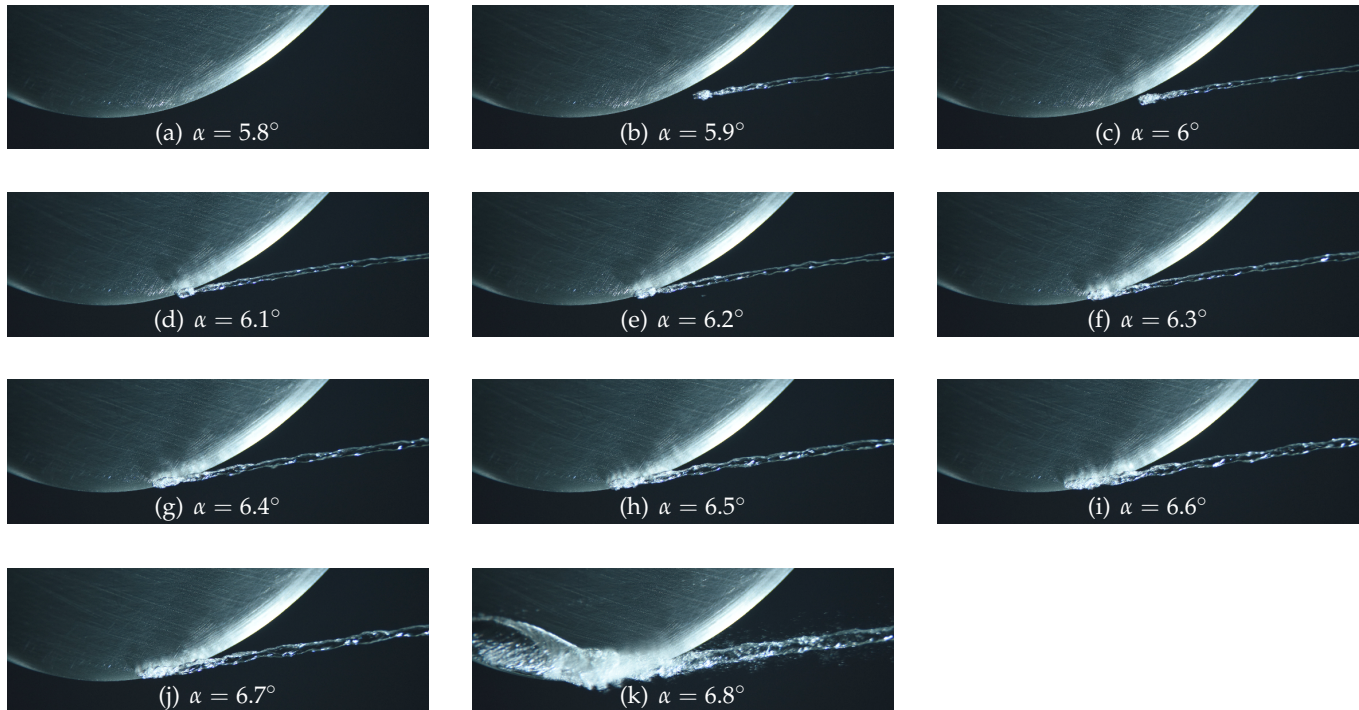


Figure 6: Photographs showing the development of trailing-vortex cavitation with increasing incidence (α).

As the incidence was increased (figures 6(c) through 6(j)), the hydrofoil generated more lift (linearly with incidence), which strengthened the trailing vortex, and thus reduced the pressure. The cavity diameter increased with the reduction in pressure, and developed more perturbations in the diameter. The diameter was measured from the photographs at several positions downstream of the tip and is presented as distributions in figure 7. The broadening of the distribution with increasing incidence is due to a twisting of the vortex. This twist is a spatial, rather than temporal, instability. That is, the vortex twists along its longitudinal axis, but this twist does not move in time. Figure 8 shows twelve uncorrelated photographs of the cavitating vortex at an incidence of 6.5° . The locations of the twists can be seen to be stable between the photographs, described as the stationary oscillation mode in Pennings *et al.* (2015) or the 'twisted ribbon' of Arndt *et al.* (1991).

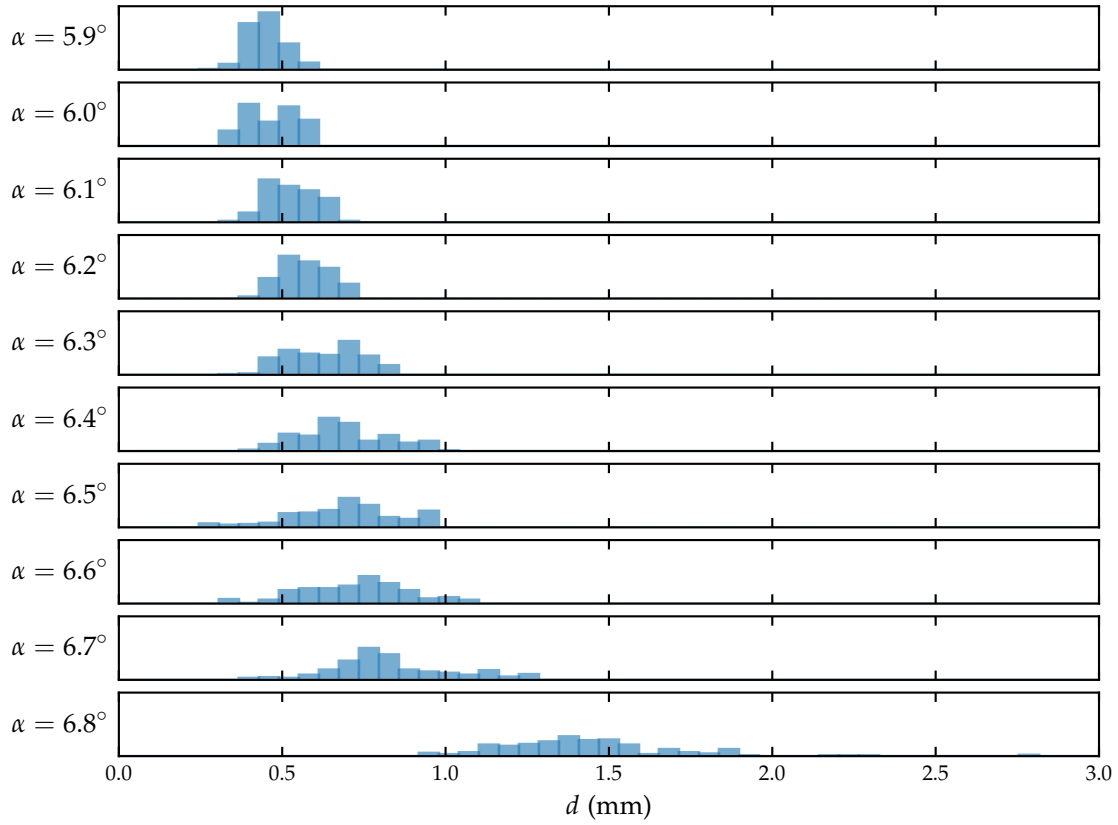


Figure 7: Distributions of the diameter (d) of the cavitating trailing vortex as the incidence (α) is varied.

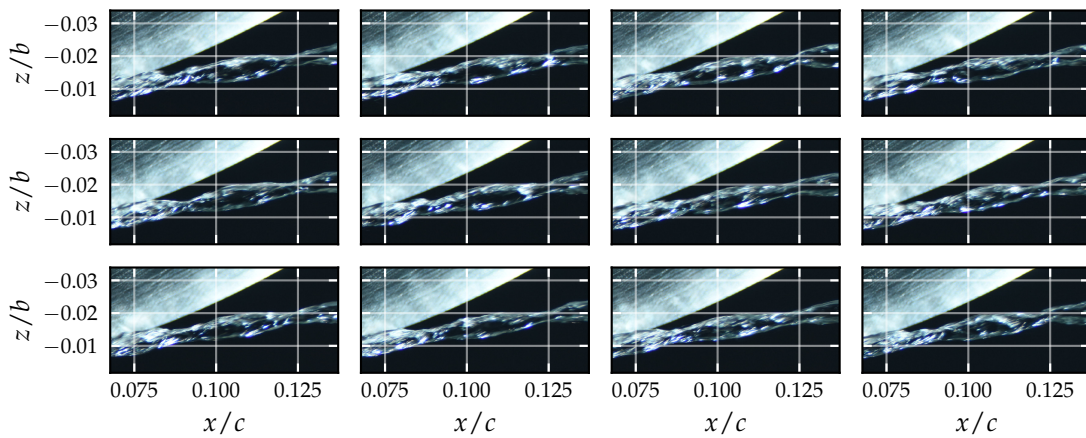


Figure 8: Photographs of the cavitating trailing vortex at different time intervals during the experiment showing the stability of the vortex twist at an incidence of 6.5° . The spatial coordinate system (x, z) is relative to the tip of the hydrofoil and is non-dimensionalised by the root chord (c) and the half-span (b).

At an incidence of 6.8° , the trailing-vortex cavitation attached to the tip of the hydrofoil and a leading-edge cavity was formed on the hydrofoil (left side of figure 6(k)). The cavity thickened to 1.4 mm diameter, and became more unstable, seen as an increase in the spread of the diameter histogram in figure 7.

Acoustic spectra of the cavitation and fluid noise is given in figure 9. These spectra have been filtered with one-third octave band filters. For the single-phase (non-cavitating, black), the spectrum exhibits peaks at 400 Hz, 730 Hz and 2.9 kHz. At the inception angle ($\alpha = 5.9^\circ$, dashed line), the spectrum increased for all frequencies above 600 Hz, and an additional spectral peak appeared at 1.2 kHz which is associated with the cavitation noise. The frequency of this peak reduced as the incidence was increased (figure 10). When the leading-edge cavitates at $\alpha = 6.8^\circ$ (red in figure 9), the noise increased by 20 dB/Hz at 650 Hz, associated with shedding near the leading edge.

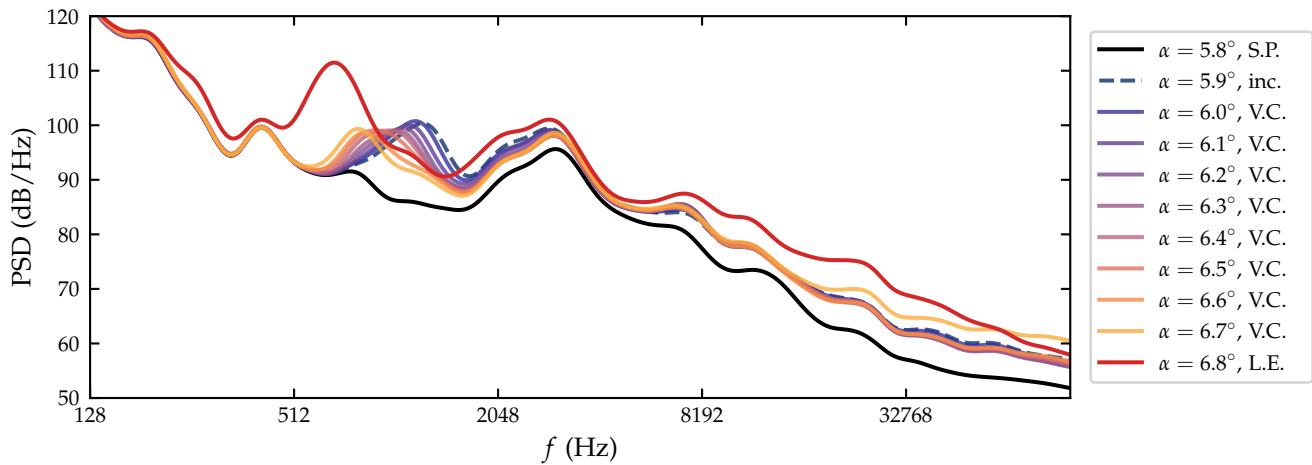


Figure 9: Acoustic spectra created by the hydrofoil at a range of cavitation conditions from single-phase (S.P.), through trailing-vortex cavitation (V.C.), with the initial inception incidence marked as ‘inc.’, and leading-edge cavitation (L.E.).

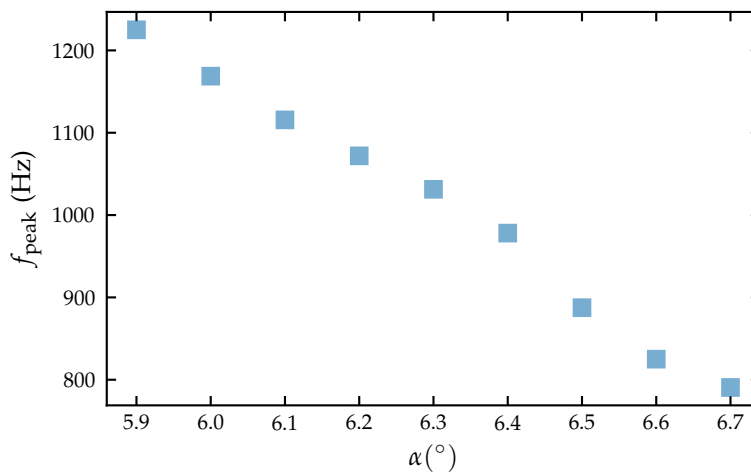


Figure 10: Peak frequency (f_{peak}) of the cavitating noise spectra for various incidences (α) during trailing-vortex cavitation development.

The overall sound-pressure level (defined as the integral of the spectra in figure 9 for all frequencies above 400 Hz), is given in figure 11, showing an initial increase of 3 dB in the noise at inception, followed by a reduction in the noise as the cavitation moves closer to the tip, and then a further increase by 5 dB in the noise when the leading-edge cavitates.

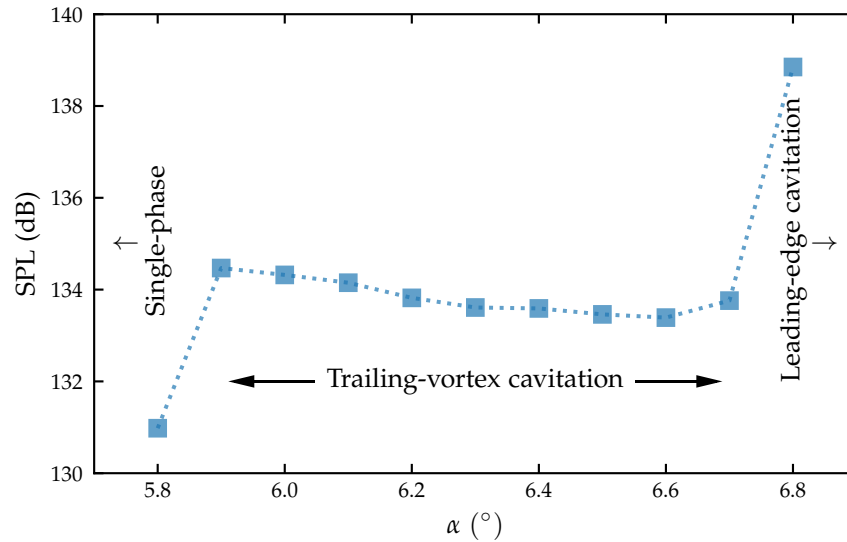


Figure 11: Sound Pressure Level (SPL) as it varies with incidence (α).

IV. CONCLUSIONS

Acoustic and photographic measurements have been made on the flow around an elliptical hydrofoil under various cavitation conditions. Inception occurs at an incidence of 5.9° . The cavity then grows with incidence and moves upstream, until the cavity combines with a leading-edge cavity on the hydrofoil. The acoustics are multi-modal with the cavitation noise associated with a peak frequency linearly reducing with incidence. The cavitation inception causes a 3 dB increase in the overall sound pressure level, and a further 5 dB increase when leading-edge cavitation occurs. These measurements provide a better understanding of the physics of trailing-vortex cavitation, which will aid in the evaluation and design assurance of marine platform propellers and control surfaces.

REFERENCES

- ARNDT, R. E. A. 2002 Cavitation in vortical flows. *Annual Review of Fluid Mechanics* **34**, 143–175.
- ARNDT, R. E. A., ARAKERI, V. H. & HIGUCHI, H. 1991 Some observations of tip-vortex cavitation. *Journal of Fluid Mechanics* **229**, 269–289.
- BRANDNER, P. A., VENNING, J. A. & PEARCE, B. W. 2018 Wavelet analysis techniques in cavitating flows. *Philosophical Transactions of the Royal Society A* **376**.
- BRENNEN, C. E. 2014 *Cavitation and Bubble Dynamics*. Cambridge University Press.
- GINDROZ, B., BILLARD, J.-Y. & GEISTDOERFER, P. 1995 Cavitation nuclei measurements at sea. In *Proceedings of the ASME Heat Transfer and Fluids Engineering Divisions*, pp. 497–503.
- GIOSIO, D., PEARCE, B. W. & BRANDNER, P. A. 2016 Influence of Pressure on Microbubble Production Rate in a Confined Turbulent Jet. In *20th Australasian Fluid Mechanics Conference*. Perth.
- KHOO, M. T., VENNING, J. A., PEARCE, B. W. & BRANDNER, P. A. 2018 Nucleation Effects on Hydrofoil Tip Vortex Cavitation. In *21st Australasian Fluid Mechanics Conference*.

- KHOO, M. T., VENNING, J. A., PEARCE, B. W., BRANDNER, P. A. & LECOFFRE, Y. 2016 Development of a Cavitation Susceptibility Meter for Nuclei Size Distribution Measurements. In *20th Australasian Fluid Mechanics Conference*.
- O'HERN, T. J., D'AGOSTINO, L. & ACOSTA, A. J. 1988 Comparison of holographic and coulter counter measurements of cavitation nuclei in the ocean. *J. Fluids Engineering* **110** (June 1988), 200–207.
- PENNINGS, P., BOSSCHERS, J., WESTERWEEL, J. & VAN TERWISGA, T. 2015 Dynamics of isolated vortex cavitation. *Journal of Fluid Mechanics* **778**, 288–313.
- RUSSELL, P. S., GIOSIO, D. R., VENNING, J. A., PEARCE, B. W. & BRANDNER, P. A. 2016 Microbubble Generation from Condensation and Turbulent Breakup of Sheet Cavitation. In *31st Symposium on Naval Hydrodynamics*. Monterey.
- RUSSELL, P. S., GIOSIO, D. R., VENNING, J. A., PEARCE, B. W., BRANDNER, P. A., AUMELAS, V. & MAJ, G. 2018 Towards real-time optical measurement of microbubble content in hydrodynamic test facilities. In *Proceedings of the 10th International Symposium on Cavitation (CAV2018)*, pp. 1056–1061. Baltimore.
- SHEN, Y. T. & GOWING, S. 1986 Cavitation susceptibility of ocean and laboratory water. In *Proceedings of the Twenty-first American Towing Tank Conference*, pp. 439–449.
- VENNING, J., GIOSIO, D., SMITH, S., PEARCE, B. & BRANDNER, P. 2018a The Influence of Nucleation on the Spectral Content of Cloud Cavitation About a Hydrofoil. In *Proceedings of the 10th International Symposium on Cavitation (CAV2018)*, pp. 1025–1030. Baltimore.
- VENNING, J. A., KHOO, M. T., PEARCE, B. W. & BRANDNER, P. A. 2018b Background nuclei measurements and implications for cavitation inception in hydrodynamic test facilities. *Experiments in Fluids* **59** (4), 1–4.
- VENNING, J. A., VINCENTIS, S. D., PEARCE, B. W. & BRANDNER, P. A. 2016 Microbubble generation for PIV seeding . In *20th Australasian Fluid Mechanics Conference*. Perth.
- WELCH, P. 1967 The use of fast Fourier transform for the estimation of power spectra: a method based on time averaging over short, modified periodograms. *IEEE Transactions on audio and electroacoustics* **15** (2), 70–73.
-